Supporting information for: Chasing Aqueous Biphasic Systems from simple salts by exploring the LiTFSI / LiCl / H_2O phase diagram

Nicolas Dubouis, Chanbum Park, Michaël Deschamps, Soufiane Abdelghani-Idrissi, Matej Kanduč, Annie Colin, Mathieu Salanne, Joachim Dzubiella*, Alexis Grimaud*, Benjamin Rotenberg*

Table of contents

Experimental Procedures and Simulation Details

MD simulations

All-atom molecular dynamics (MD) simulations are carried out with the GROMACS 5.1 simulation package.[1] Initially, two independent simulation boxes for LiCl+water and LiTFSI+water are prepared with the PACKMOL package[2] according to the concentrations of interest. The sizes of the simulation box and numbers of species are summarized in Table S1. The initial configurations in the simulation boxes are first relaxed by minimizing the potential energy using steepest descent and then the two independent simulation boxes are merged into a single simulation box. For the equilibration and production runs, the simulation boxes are maintained at an isotropic pressure of 1 bar with the Parrinello-Rahman barostat[3] and the temperature at 298 K with a velocity rescaling thermostat.[4] We monitor the density profiles for ions and water molecules until the profiles are converged (see Table S1 for the duration of the equilibration and production runs). The density profiles reported in the figures correspond only to the production runs. Periodic boundary conditions are applied in all three spatial directions. Non-bonded interatomic interactions are described by a 6–12 Lennard-Jones potential with a cut-off at 1.2 nm. The Particle-Mesh-Ewald (PME) method[5] with a Fourier spacing of 0.12 nm and a 1.2 nm real-space cut-off is used to calculate electrostatic interactions. The LINCS algorithm[6] is employed for all bond constraints. The OPLS-AA force field[7] is used for Li^+, Cl^- and the CL & P force field[8] is employed for $TFSI^-$. The SPC/E model is used for the water molecules.[9]

Table S1. Simulation box sizes, duration of the production run and numbers of ions/molecules in MD simulations.

System	Equilibrium box lengths (nm) X x Y x Z	Equilibration & Production runs (ns)	Number of ions/molecules			
			Li^+	Cl^-	$TFSI^-$	Water
1m+1m	4.2 x 4.2 x 21.0	100 & 400	400	200	200	10746
4m+4m	4.2 x 4.2 x 30.2	500 & 230	1600	800	800	10746
6m+6m	4.2 x 4.2 x 35.9	500 & 180	2340	1170	1170	10746
12m+5m	9.1 x 9.0 x 26.2	200 & 160	11137	7937	3200	35988

Materials

All the chemicals, such as lithium bis(trifluoromethanesulfonyl)imide (Solvay), lithium chloride (Alfa Aesar, 98+%) are used as received. Ultrapure Mili-Q water is used in all the experiments.

Solution preparation

Solutions are prepared by mixing the two salts in a vial. The right amount of water is added to reach the target final composition.

Optical Microscopy

Movies of the drop of 5m LiTFSI in 18m LiCl were recorded by injecting with a syringe a drop of about 10 µL. The total magnification is x12.5.

Liquid-state Nuclear Magnetic Resonance Imaging

Liquid-state NMR spectra are recorded on a Bruker 4.7 T Avance HD spectrometer mounted with a Diff-30 Z-gradient probehead. ^1H and ^7Li mapping of the tubes are recorded using a 1D Chemical Shift Imaging (CSI) sequence with 4 transients and 128 gradient increments. The gradient pulse was 1 ms long, with a maximum gradient strength of 20.2 G/cm for ^7Li and 7.9 G/cm for ^1H, corresponding to an overall field of view of 3 cm. The RF pulse strength was set to 6 kHz for ^1H and 15.6 kHz for ^7Li, and the recycle delays were set to 1s in both cases. The concentration profiles for ^1H, ^7Li

and ^{19}F are obtained using a direct acquisition under a small constant gradient. The full echo signal is recorded with an echo sequence ("improf" in Bruker spectrometers), with a 90° pulse followed by a short gradient pulse during the first echo delay, and after a refocusing 180° pulse, the gradient is switched on and the full echo FID is recorded. The parameters used are shown in the table below for each nucleus:

Table S2: NMR parameters used for the concentration profiles.

Nucleus	Transients number	Recovery delay	RF strength	Gradient strength
^{1}H	32	3 s	6 kHz	12 G/cm
^{19}F	128	1 s	7.4 kHz	12 G/cm
^{7}Li	16	10 s	15.6 kHz	12 G/cm

The excited zone corresponds to the liquid inside the NMR coil, which is roughly 2.5-3 cm high. The longitudinal relaxation times (T_1) of each species have been measured to ensure quantitative measurements.

Table S3: Longitudinal relaxation times (T_1) measured for the different species in the 12m LiCl - 5m LiTFSI system

Phase	^{1}H	^{19}F	^{7}Li
$LiTFSI.H_2O$	667 ms	631 ms	366 ms
$LiCl.H_2O$	510 ms	859 ms	1.943 s

It must be noted that a small amount of TFSI was detected in the LiCl phase in the 1D spectrum, and its peak is weaker by a factor of around 760. A similar ratio (1/740) is observed in the 1D concentration profile (detail not shown).

Fourier-Transform Infrared Spectroscopy

FTIR spectra are recorded on a Nicolet iS5 FTIR spectrometer, mounted with a diamond Attenuated Total Reflectance accessory (iD1 ATR). One drop of the solution was analyzed using 16 scans with a 4 cm^{-1} resolution from 4 000 to 500 cm^{-1}. The background correction is performed by measuring the ambient atmosphere under the same conditions as for the solutions measured in this work**.**

Phase-diagram construction

The phase diagram is constructed using the point-cloud titration method.[10] Briefly, a precise mass of a concentrated solution of LiTFSI (20 m) or LiCl (18 m) is introduced in a test tube, which was weighted (m_I). The other solution is introduced dropwise, until a cloudy solution is observed. The tube is weighted again (m_c) so that the mass of the added solution can be deduced ($m_S=m_c-m_I$) and the composition of the system is reported as a point of coexistence (biphasic system). Then, water is added dropwise until the solution turns limpid. The tube is then weighted (m_L) to determine the mass of added water ($m_W=m_L-m_C$) and the point corresponding to the monophasic system is reported on the phase diagram. To ensure a proper determination of the required number of drops, the solution is vortexed after every drop addition. To study the system for a large range of compositions, the titration was carried out starting either from a stock solution of LiTFSI or LiCl. The proper junction between the two series of measurements observed in the phase diagram (Figure 3, main text) validates the accuracy of the method.

Viscosity measurements

Viscosity measurements are carried out on a Discovery HR-2 (TA instruments) rheometer using a Peltier concentric cylinders geometry at 25 °C (controlled temperature, +/- 0.2 °C). Kinematic viscosity is measured for shear rates between 1.0 $s^{-1}$and 30.0 s^{-1}. Retained values for the viscosity resulted from the average of 5 measurements recorded with shear rates comprised between 12.6 s^{-1} and 30 s^{-1}. Error bars are calculated from the standard deviation of the 5 measurements with the average value.

Surface-tension measurement

Surface tension measurement between liquids is performed using an automatic tensiometer (Tracker- Single drop).

Electrochemical measurements

Dual ion batteries using Mo_6S_8 as lithium insertion electrode and polypyrrole as chlorine insertion electrode are prepared and assembled as follows. Mo_6S_8 is obtained by leaching $Cu_2Mo_6S_8$ in a 6 M HCl aqueous solution under oxygen.[11] $Cu_2Mo_6S_8$ is prepared by a solid-state synthesis method (elemental precursors are introduced in a stoichiometric amount in a glass tube, which is sealed under vacuum and heated up at 1100 °C for 72h). Self-standing electrodes are prepared by mixing in acetone Mo_6S_8 powder with carbon super-P, PVDF, and dibutylphtalate (DBP) in the following weight ratios: 100/12.5/25/40. The as prepared slurry is spread in a petri-dish. Once the acetone is evaporated, half-inch electrodes are punched from the film. DBP is removed from the electrodes by washing them 3 times for 30 minutes in diethylether. Electrodes are dried under vacuum overnight at room temperature. Polypyrrole (PP) electrodes are obtained by electropolymerizing pyrrole (Alfa, 98+%) in 1.2 M HCl on a carbon paper, as described elsewhere.[12] Before use, PP electrodes are dechlorinated by holding them at -0.840 V vs a Saturated Calomel Electrode (SCE) in a 1m LiCl solution. Plastic Swagelok cells with a PTFE-disk spacer are assembled by placing the Mo_6S_8 electrode on the bottom plunger, adding first the 20 m LiTFSI and then the 18 m LiCl solution. The polypyrrole electrode – soaking only in the LiCl electrolyte – is then placed on the top of the PTFE-disk spacer and is directly in contact with the top plunger. A scheme of the assembly is represented below. As made Swagelok cells are cycled on a VMP3 potentiostat from Biologic.

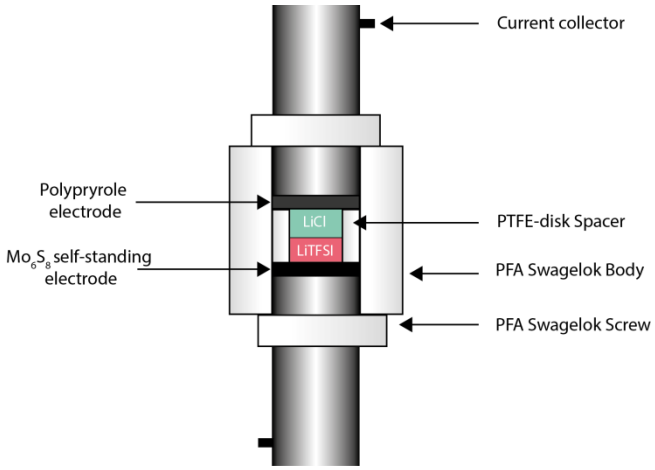

Scheme S1. Custom Swagelok cell used to cycle the ABS dual ion battery.

Results and Discussion

S1. Photography of drop of LiTFSI in LiCl aqueous solutions

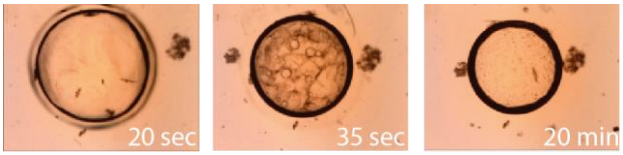

Figure S1. Optical microscopy images showing the evolution over time of a ~ 10 µL drop of 5 m LiTFSI solution in 18 m LiCl solution.

The decrease of the drop diameter reveals a mass transfer from the 5 m LiTFSI phase to the 18 m LiCl solution, which could be attributed to a transfer of water. After 20 minutes, no further evolution was observed. This confirms the formation of a stable ABS even for small volumes.

S2. Concentration profiles calculated from MD simulations with different global compositions

Figure S2. Concentration profiles obtained by Molecular Dynamics simulations for the 1m-1m (A), 4m-4m (B), and 6m-6m (C) systems. Snapshots of the simulations are also shown, with Cl^- anions in green, $TFSI^-$ anions in red, and Li^+ cations in orange (water not shown).

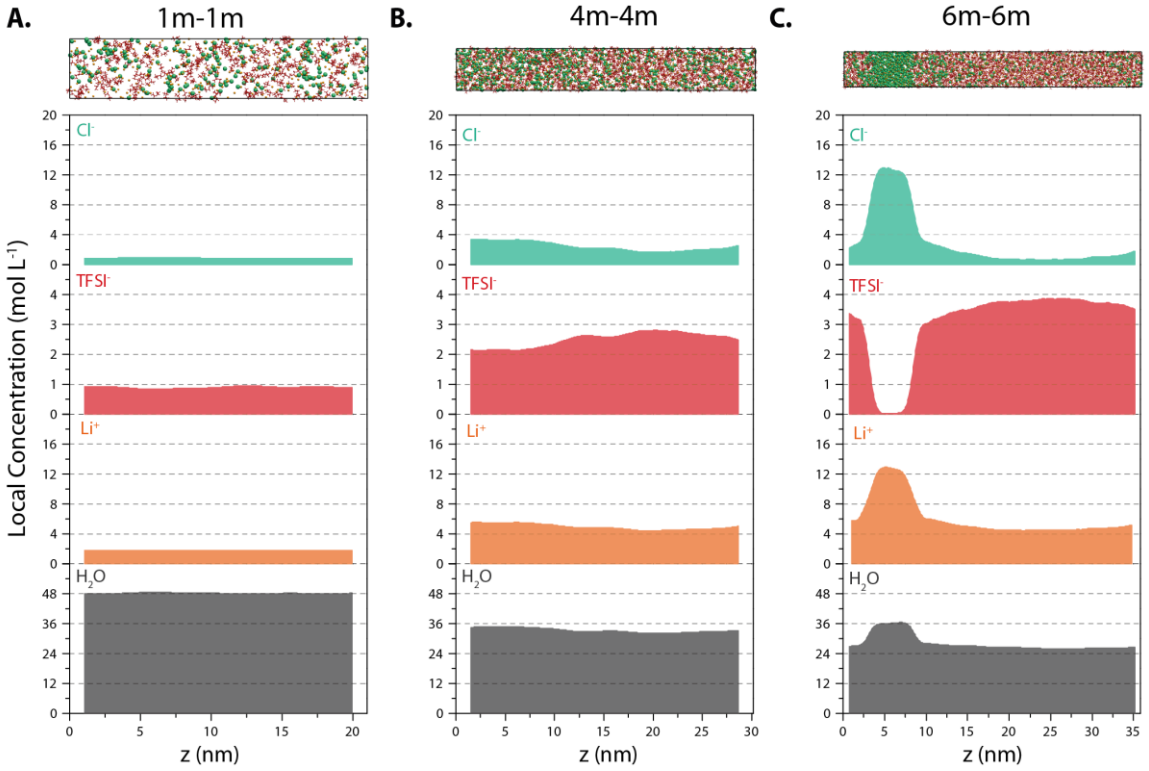

While the systems are clearly monophasic for 1m LiCl – 1m LiTFSI and biphasic for 6m–6m, the 4m–4m system does not show sharp interfaces, even though the density profiles are reasonably converged. The composition of each phase of the ABS (as reported by full symbols in Figure 3 of the manuscript) is computed from these density profiles as averages in the corresponding regions, summarized in Table S4.

Table S4. Regions used to compute the composition of each phase from the density profiles (Figure 2 of the manuscript for the 12m–5m system, S2B for 4m–4m and S2C for 6m–6m).

System	Region for Cl-rich phase (nm)	Region for TFSI-rich phase (nm)
12m–5m	4.3 to 9.3	17.5 to 22.5
4m–4m	2 to 7	13.5 to 25
6m–6m	4.7 to 7.2	18 to 29

S3. Solvation of Li^+ cations in the LiCl and LiTFSI rich phases

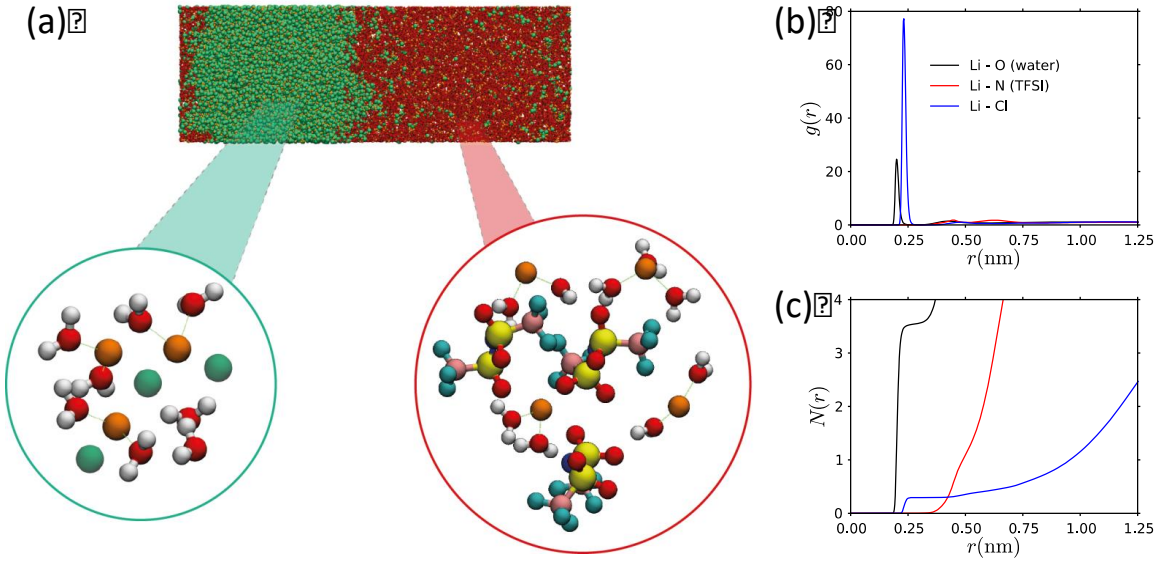

Figure S3. (a) MD snapshot of the 12m LiCl – 5m LiTFSI system, showing the solvation structures of Li^+ cations (orange) in the LiCl (Cl^- in green in top panel and bottom left panel) and LiTFSI ($TFSI^-$ in red in top panel, with separate colors for each atom in bottom right panel) rich phases. Li^+ cations remain partially solvated by water molecules (O in red, H in white) in both phases. (b) Radial distributions around Li^+ cations in the TFSI-rich phase. (c) Running coordination numbers around Li^+ cations in the TFSI-rich phase.

The Li^+ cations are solvated by water molecules in both phases, as illustrated in Figure S3a. In order to investigate quantitatively the environment of the cations in the TFSI-rich phase of the ABS formed in the 12m LiCl – 5m LiTFSI system, we conducted additional molecular dynamics simulations of a bulk system with the same composition. Specifically, the system consists of 1956 Li^+, 1956 $TFSI^-$, 200 Cl^-, and 10038 water molecules in a cubic box. The molecules are inserted into the simulation box randomly using the PACKMOL package and relaxed with the steepest descent algorithm. After a simulated annealing from 500 K down to 298 K within a time interval of 3 ns in the NVT ensemble, the system is compressed in the NPT ensemble at 50 bar and 298 K for 1.5 ns. After further equilibration for 5 ns at 1 bar (the equilibrated box length is L=8.86 nm), we perform a 96 ns production run at 1 bar, from which we compute the radial distribution functions, g(r), between Li^+ cations, water O atoms, TFSI N atoms, and Cl^- anions. They are reported in Figure S3b, which clearly shows that the direct environment of the Li^+ cations consists essentially of water molecules and Cl^- anions. Despite the larger peak for the latter, the first coordination shell of the cations mainly consists of water, which is present in much larger quantities than Cl^- in the TFSI-rich phase. This is obvious in Figure S3c, which shows the running coordination numbers $N(r) = \int_0^r \rho g(r') 4\pi (r')^2 dr'$ with ρ being the density of the species of interest. The plateaus at around 0.3 nm indicate that there are on average almost no TFSI, 3.6 water molecules, and 0.3 Cl^- anions in the first coordination shell of Li^+.

S4. Viscosity measurements and Jones-Dole coefficients for LiTFSI, LiCl, and KCl aqueous solutions

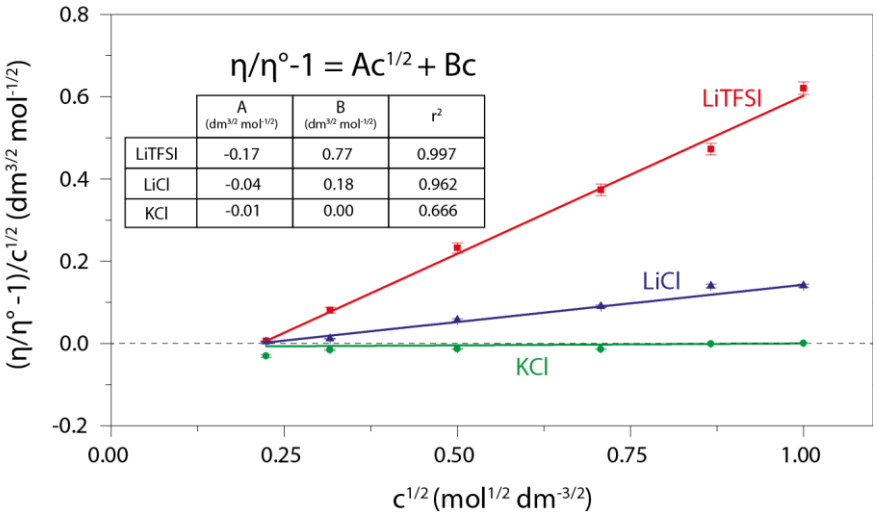

	A ($dm^{3/2}$ $mol^{-1/2}$)	B ($dm^{3/2}$ $mol^{-1/2}$)	r^2
LiTFSI	-0.17	0.77	0.997
LiCl	-0.04	0.18	0.962
KCl	-0.01	0.00	0.666

Figure S4. Viscosity measurements for low concentrations (0 to 1 mol L^{-1}) aqueous solutions of LiTFSI (red), LiCl (blue) and KCl (green). Straight lines represent a linear fitting with the Jones-Dole equation.

As described in the main manuscript, the formation of an ABS using different salts was explained in the literature to result from the presence of water structuring (kosmotropic) ions in one phase and disorder-making (chaotropic) ions in the other phase. A common way to assess effect of individual ions on water structure is to measure the viscosity of dilute solutions (from 5 mM to 500 mM) and to determine the B-coefficient in the Jones-Dole equation ($\eta/\eta_{water} - 1 = Ac^{1/2} + Bc$) by comparing with the results obtained for KCl, assuming the additivity of ionic contributions (and using the fact that $B_{K+} = -B_{Cl-}$, see below).[13,14] The viscosity measured for LiTFSI, LiCl, and KCl solutions from 50 mM to 1 M are well described by the Jones-Dole equation for the three salts, which allows us to determine the corresponding A and B parameters. An almost null B-coefficient is measured for KCl, for which it can be deduced $B_{K+} = -B_{Cl-} = 0.00$ $dm^{3/2}$ $mol^{-1/2}$. The positive B-coefficient of +0.18 $dm^{3/2}$ $mol^{-1/2}$ found for Li^+ cations indicates its water-structuring role (kosmotropic) and is in excellent agreement with the literature (+0.15 $dm^{3/2}$ $mol^{-1/2}$ in reference 12). Finally, the B-coefficient for $TFSI^-$ anions of +0.59 $dm^{3/2}$ $mol^{-1/2}$ can be deduced from the slope obtained for LiTFSI and the above value for Li^+. As discussed in the main text, such positive coefficients may indicates a kosmotropic effect for $TFSI^-$ anions, which may seem counter-intuitive based on previous reports.[15,16] From reference 13, it can be concluded that this positive coefficient is rather due to the large size and hydrophobic character of $TFSI^-$ anions.

S5. Dual ion battery using the ABS as electrolyte

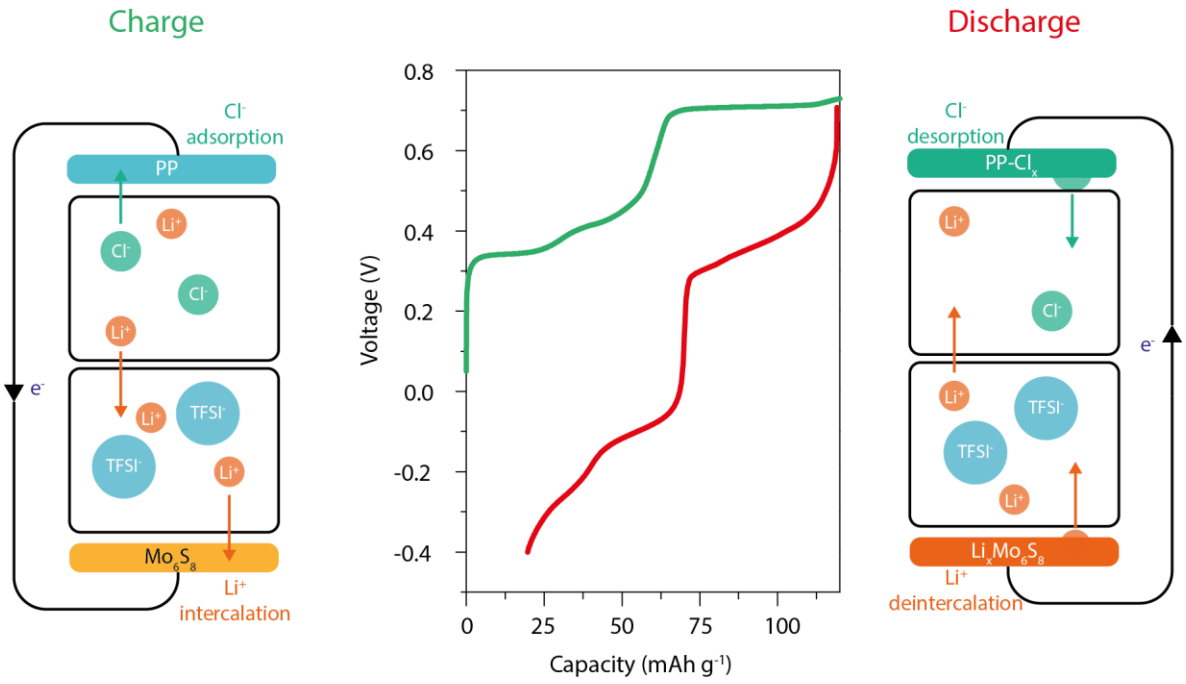

Figure S5. First charge (green) and discharge (red) cycle obtained for a dual ion battery using a 20m LiTFSI-18m LiCl ABS electrolyte with a polypyrrole chlorine adsorption positive electrode and a Mo_6S_8 negative electrode. Capacity is expressed based on the Mo_6S_8 mass. Cycling was done at a C rate of 1 (1 mol of electron per hour), based on Mo_6S_8 mass.

This experiment confirms the possibility of using ABS to develop dual ion batteries with different anolytes and catholytes in absence of any membrane. The "water-in-salt" electrolyte (20 m LiTFSI) allows the cycling of Mo_6S_8 in aqueous electrolyte[17], while the 18 m LiCl electrolyte allows the PP electrode to work as a pseudo-capacitor for Cl^- ions.[12] In particular, the interface between the two phases remains stable even when an electric field is applied. Further improvements, such as stability of the positive current collector in presence of Cl^- and reducing the large hysteresis observed in this preliminary experiment, would be required to assemble a practical dual ion battery based on ABS electrolytes.

Supporting Information References

(1) Spoel, D. V. D.; Lindahl, E.; Hess, B.; Groenhof, G.; Mark, A. E.; Berendsen, H. J. C. GROMACS: Fast, Flexible, and Free. *Journal of Computational Chemistry* **2005**, *26* (16), 1701–1718. https://doi.org/10.1002/jcc.20291.

(2) Martínez, L.; Andrade, R.; Birgin, E. G.; Martínez, J. M. PACKMOL: A package for building initial configurations for molecular dynamics simulations. *Journal of Computational Chemistry* **2009**, *30* (13), 2157–2164. https://doi.org/10.1002/jcc.21224.

(3) Parrinello, M.; Rahman, A. Polymorphic Transitions in Single Crystals: A New Molecular Dynamics Method. *Journal of Applied Physics* **1981**, *52* (12), 7182–7190. https://doi.org/10.1063/1.328693.

(4) Bussi, G.; Donadio, D.; Parrinello, M. Canonical Sampling through Velocity Rescaling. *J. Chem. Phys.* **2007**, *126* (1), 014101. https://doi.org/10.1063/1.2408420.

(5) Darden, T.; York, D.; Pedersen, L. Particle Mesh Ewald: An N·log(N) Method for Ewald Sums in Large Systems. *J. Chem. Phys.* **1993**, *98* (12), 10089–10092. https://doi.org/10.1063/1.464397.

(6) Hess, B. P-LINCS: A Parallel Linear Constraint Solver for Molecular Simulation. *J. Chem. Theory Comput.* **2008**, *4* (1), 116–122. https://doi.org/10.1021/ct700200b.

(7) Jorgensen, W. L.; Maxwell, D. S.; Tirado-Rives, J. Development and Testing of the OPLS All-Atom Force Field on Conformational Energetics and Properties of Organic Liquids. *J. Am. Chem. Soc.* **1996**, *118* (45), 11225–11236. https://doi.org/10.1021/ja9621760.

(8) Canongia Lopes, J. N.; Pádua, A. A. H. Molecular Force Field for Ionic Liquids Composed of Triflate or Bistriflylimide Anions. *J. Phys. Chem. B* **2004**, *108* (43), 16893–16898. https://doi.org/10.1021/jp0476545.

(9) Berendsen, H. J. C.; Grigera, J. R.; Straatsma, T. P. The Missing Term in Effective Pair Potentials. *J. Phys. Chem.* **1987**, *91* (24), 6269–6271. https://doi.org/10.1021/j100308a038.

(10) Gutowski, K. E.; Broker, G. A.; Willauer, H. D.; Huddleston, J. G.; Swatloski, R. P.; Holbrey, J. D.; Rogers, R. D. Controlling the Aqueous Miscibility of Ionic Liquids: Aqueous Biphasic Systems of Water-Miscible Ionic Liquids and Water-Structuring Salts for Recycle, Metathesis, and Separations. *J. Am. Chem. Soc.* **2003**, *125* (22), 6632–6633. https://doi.org/10.1021/ja0351802.

(11) Lancry, E.; Levi, E.; Gofer, Y.; Levi, M.; Salitra, G.; Aurbach, D. Leaching Chemistry and the Performance of the Mo6S8 Cathodes in Rechargeable Mg Batteries. *Chem. Mater.* **2004**, *16* (14), 2832–2838. https://doi.org/10.1021/cm034944+.

(12) Missoni, L. L.; Marchini, F.; Pozo, M. del; Calvo, E. J. A LiMn2O4-Polypyrrole System for the Extraction of LiCl from Natural Brine. *J. Electrochem. Soc.* **2016**, *163* (9), A1898–A1902. https://doi.org/10.1149/2.0591609jes.

(13) Jenkins, H. D. B.; Marcus, Y. Viscosity B-Coefficients of Ions in Solution. *Chemical reviews* **1995**, *95* (8), 2695–2724.

(14) Marcus, Y. Effect of Ions on the Structure of Water: Structure Making and Breaking. *Chemical Reviews* **2009**, *109* (3), 1346–1370. https://doi.org/10.1021/cr8003828.

(15) Su, H.-L.; Lan, M.-T.; Lin, K.-W.; Hsieh, Y.-Z. Chaotropic Salts: Novel Modifiers for the Capillary Electrophoretic Analysis of Benzodiazepines. *ELECTROPHORESIS* **2008**, *29* (16), 3384–3390. https://doi.org/10.1002/elps.200800073.

(16) Giammanco, C. H.; Kramer, P. L.; Fayer, M. D. Ionic Liquid versus Li^+ Aqueous Solutions: Water Dynamics near Bistriflimide Anions. *The Journal of Physical Chemistry B* **2016**, *120* (37), 9997–10009. https://doi.org/10.1021/acs.jpcb.6b07145.

(17) Suo, L.; Borodin, O.; Gao, T.; Olguin, M.; Ho, J.; Fan, X.; Luo, C.; Wang, C.; Xu, K. "Water-in-Salt" Electrolyte Enables High-Voltage Aqueous Lithium-Ion Chemistries. *Science* **2015**, *350* (6263), 938–943. https://doi.org/10.1126/science.aab1595.

Author Contributions

ND prepared the solutions, conducted the FTIR experiments, performed the electrochemical measurements and realized the phase diagram**.** AG and ND analyzed those experimental results. SAI and ND measured the viscosity and followed the evolution of the ABS by microscopy, these results were further analyzed by AC. MD conducted and analyzed NMR measurements. BR, JD and MS designed the simulations, which were performed by CP and MK and analyzed by all 5. ND and CP produced the figures; all authors contributed to writing the manuscript under the coordination of the corresponding authors.